Research Square

Preprints are preliminary reports that have not undergone peer review.
They should not be considered conclusive, used to inform clinical practice,
or referenced by the media as validated information.

Mapping postglacial succession of coniferous tree species in high elevation ecosystems of British Columbia

Edward Anderson
Simon Fraser University, School of Environmental Science
Courtney G. Collins
courtney.collins@gov.bc.ca

British Columbia Ministry of Forests, Forest Carbon and Climate Services Branch,
https://orcid.org/0000-0001-5455-172X
Cassandra Elphinstone
University of British Columbia, Department of Botany
Ciara Norton
University of British Columbia, Faculty of Forestry
Sebastian Yerex
University of Victoria, Department of Geography
Shawn Chartrand
Simon Fraser University, School of Environmental Science

Research Article

Keywords: glacial retreat, forest succession, multispectral and hyperspectral imagery, conifer, british columbia

Posted Date: September 18th, 2025

DOI: https://doi.org/10.21203/rs.3.rs-7633992/v1

License: This work is licensed under a Creative Commons Attribution 4.0 International License.
Read Full License

Additional Declarations: The authors declare no competing interests.

Title: Mapping postglacial succession of coniferous tree species in high elevation ecosystems of British Columbia

Authors: Edward Anderson[a], Courtney G. Collins[a,b,c] , Cassandra Elphinstone[c] , Ciara Norton[d], Sebastian Yerex[e] and Shawn M. Chartrand[a]

Author Affiliations:

a) Simon Fraser University, School of Environmental Science, Burnaby, B.C., Canada

b) British Columbia Ministry of Forests, Forest Carbon and Climate Services Branch, Victoria, B.C., Canada

c) Department of Botany, University of British Columbia, Unceded xʷməθkʷəy̓əm (Musqueam) Territory, Vancouver, V6T 1Z4, British Columbia, Canada

d) University of British Columbia, Faculty of Forestry, Vancouver, B.C. Canada

e) University of Victoria, Department of Geography, Victoria, B.C. Canada

Draft

Abstract

In western North America, most glaciers are predicted to disappear by 2100 under a 2-3 degrees Celsius warming scenario. Despite this, little research has been done on postglacial succession in the region. To address this, we leveraged multispectral drone imagery and machine learning techniques to investigate patterns of post-glacial conifer succession in two glacial bays in Garibaldi (Nch'k̲ay̓) Provincial Park: Sphinx Bay and Sentinel Bay. We classified rasters at a 10 cm resolution using multispectral band values from ground-based training data. The random forest classification predicted subalpine fir (Abies lasiocarpa) dominated in Sentinel Bay and mountain hemlock (Tsuga mertensiana) as the dominant tree in Sphinx Bay. Higher elevations, less sun exposure, and more recent deglaciation in Sentinel Bay indicate that subalpine fir and mountain hemlock follow distinct post-glacial successional patterns, with subalpine fir more tolerant of poorly developed paraglacial soils and mountain hemlock requiring more well developed, mesic soils. These patterns confirm previously documented patterns of forest succession among these species in other areas. We found that machine learning tools can effectively be combined with drone imagery and ground surveys to map vegetation responses to deglaciation, but results can be limited by subjective photointerpretation and sparse data.

© The Author(s) or their Institution(s)

Introduction

Climate change is altering alpine ecosystems across the globe, in particular high elevation mountain ecosystems, which are warming more rapidly than lower elevations (Pepin et al 2015). As a result, mountain glaciers are retreating worldwide, with some of the most pronounced shifts occurring in Western North America (Rounce et al 2023). This pattern is expected to intensify, with almost complete deglaciation by 2100 projected for this region under a 2-3 degrees C warming scenario (Rounce et al 2023). British Columbia's (BC) mountain ecosystems contain approximately 17,000 glaciers, estimated at 3% of the total provincial land mass (Beedle & Menounos 2005). A near total loss of this glacial coverage will expose significant land area across the province to forest succession by the end of the century.

Substantial research has examined forest successional responses to other landscape level disturbances such as wildfire, insect outbreaks, or windthrow (Agee & Smith 1984, Swift & Ran 2012), as well as in contemporary glacial retreat in other parts of the world, particularly in the Alps (Ramskogler et al 2023), but less, to our knowledge, has examined similar successional responses to current or projected glacial retreat in mountain environments in Western Canada (but see Brink 1959). Due to this gap in information, we do not know whether subalpine plant species will follow similar patterns of succession in recently deglaciated areas, and what key drivers determine where these species will establish across the landscape. Given the vast glacial area found in the province, the rapid deglaciation projected by the end of the century, and the relative lack of research in this region, this highlights the need for investigation into paraglacial succession in mountainous environments in BC.

In addition, contemporary research has emphasized the role of climate warming and reduced snowpack in driving changes to elevational tree lines in high elevation forested ecosystems, (Danby & Hik 2007, Harsch et al 2009, Trant & Hermanutz 2014). Indeed, this is a well-observed phenomenon that can dramatically shift the structure and function of these (sub)alpine ecosystems. However, less research has examined the changes in forest cover or species ranges that are occurring through (current and future projected) climate driven glacial retreat. This landscape level conversion has the potential to greatly alter plant and animal community composition and diversity, as well as dramatically change ecosystem functions such as above and belowground carbon storage, hydrology and freshwater resource availability and habitat provisioning (Milner et al 2009, Fell 2017, Erica et al 2024). A large knowledge gap of vegetation-landscape interactions persists in these highly dynamic paraglacial landscapes (Klaar et al 2014), particularly in Western Canada. This may be due to a lack of overlap in methodology and questions between mountain geomorphologists and ecologists (Eichel et al 2023; but see Rice et al 2012). Nonetheless, as high elevation ecosystems continue to change at an accelerating rate, understanding the biogeomorphic patterns

© The Author(s) or their Institution(s)

and processes driving these changes will be critical for forest management, conservation, and climate change mitigation.

Recent advances in geospatial analyses provide an exciting opportunity to document and analyze underlying drivers of changes in tree species distribution and abundance in paraglacial ecosystems. Combining multiple sources of information including multispectral imagery, terrain data and/or LiDAR based information such as canopy height models with machine learning algorithms can generate a powerful workflow for distinguishing and predicting different species across a landscape (Schiefer et al 2020). Depending on the application, ground truthing data can be critical in training and calibrating model predictions. In British Columbia, forest inventories often rely on manual interpretation of aerial or satellite imagery, raising concerns regarding subjective interpretation and potentially outdated surveys (Baron et al 2024). Given limited access and surveying opportunities in remote alpine environments, it is crucial that ground truthing surveys of vegetation communities are obtained in a way that maximizes their value for different areas of research, particularly in remote sensing and analyzing vegetation changes.

This research examines forest succession in two high elevation glacial forelands of Garibaldi (Nch'k̲a̓y̓) Provincial Park in the Southern Coast Mountains of British Columbia (Figure 1). These areas (discussed under the Study Site section below) have each lost at least 1.5 km^2 of glacial ice since the 1920s (Koch et al 2009) and are presently dominated by subalpine forests of Mountain hemlock (*Tsuga mertensiana*), Subalpine fir (*Abies lasiocarpa*), and Pacific Silver fir (*Abies amabalis*), as well as species of conservation concern such as Whitebark pine (*Pinus albicaulis*). As deglaciation continues in Garibaldi (Nch'k̲a̓y̓) Provincial Park, our work attempts to better understand whether specific physiographic and environmental conditions such as topographic steepness or elevation, for example, correlate to spatial patterns of species succession on terrain of relatively recent deglaciation, as well as to use remote sensing data to attempt to better understand subalpine conifer forests in these environments.

To address these objectives, we used high resolution (10 cm) multispectral drone imagery in combination with ground truthing plant survey data to map the species and community level patterns of postglacial forest succession across two distinct glacial forelands in this region. These data were collected in the summer of 2023 from two neighboring glacial bays, each with similar histories of glacial retreat (Koch et al 2009) but with unique recolonization patterns in terms of tree species abundance and distribution. To create spatially explicit maps of species distributions across the landscape in each bay, we assigned multispectral signatures for key tree species using a supervised classification trained on ground truthing data and geomorphic properties (e.g. slope, aspect, elevation). We then used permutational variable importance to assess the key underlying drivers of different species trajectories across the landscape.

© The Author(s) or their Institution(s)

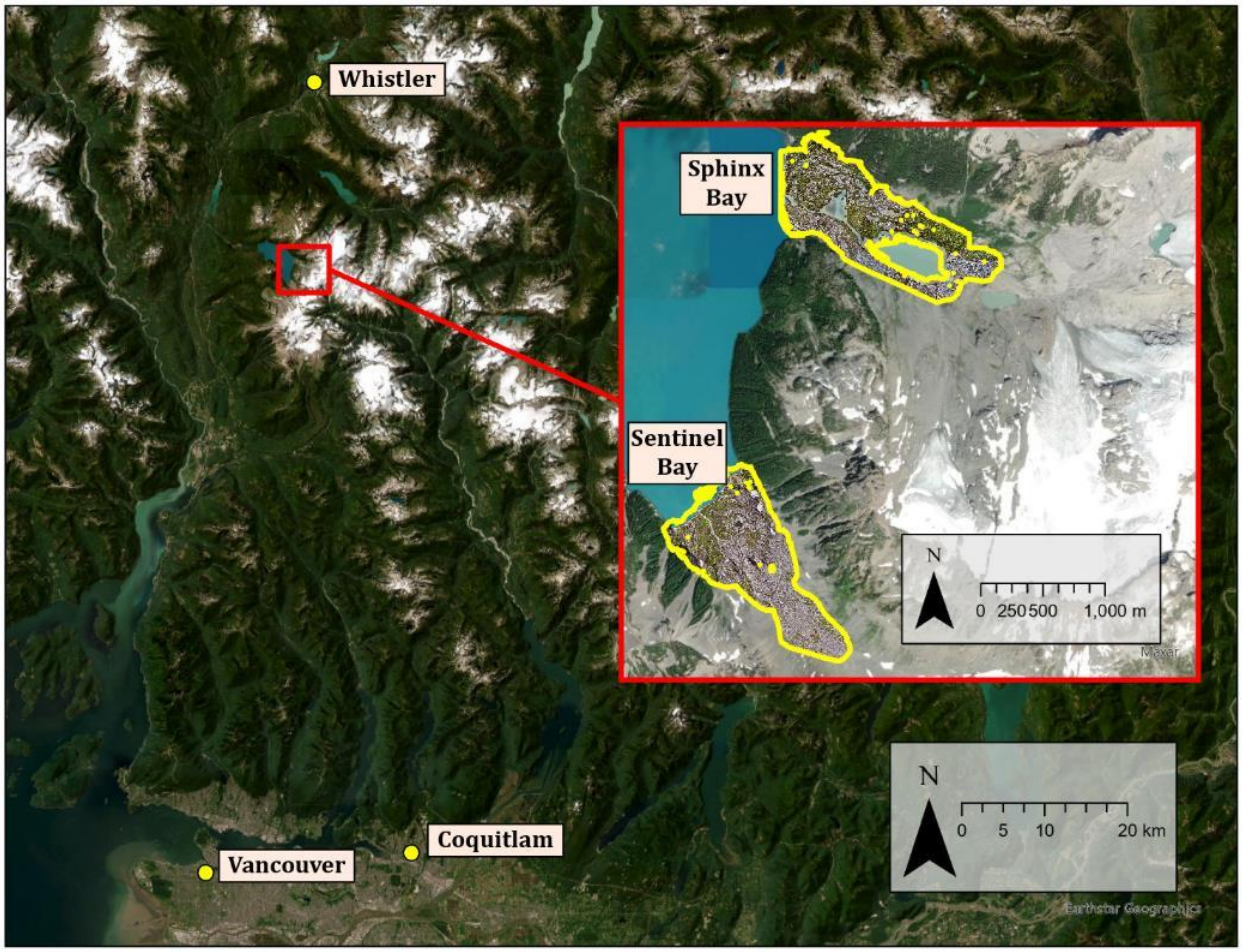


Figure 1: The location of Sentinel Bay and Sphinx Bay, approximately 70 km north of Vancouver in Garibaldi (Nch'k̲a̓y̓) Provincial Park. The coverage areas for Sentinel Bay (0.926 km^2 in the south of Garibaldi Lake) and Sphinx Bay (1.005 km^2 in the east of Garibaldi Lake) are demarcated with a yellow border.

Study Area and Methods

Study Area

This study took place within Garibaldi / Nch'k̲a̓y̓ Provincial Park, British Columbia, in two large glacial forelands of Sphinx and Sentinel Bay situated at approximately 1450-1500 m above mean sea level. This area is approximately 70 km north of Vancouver, BC in the South Coast Mountain Range, and contains some of the southernmost glaciers in British Columbia (Mood & Smith 2015) (Figure 1). Given their relatively low altitudes, and the strong coastal influence of the Pacific Ocean, the glacial landscapes and (sub)alpine ecosystems in this region are particularly vulnerable to climate change. The area around Garibaldi Lake has a diverse geological history (Mathews W.H. 1958 a,b), which has contributed to the

© The Author(s) or their Institution(s)

wide variety of plant species in this region. The glacial history has been well studied, with a focus on glacial advance and retreat since the Little Ice Age. Much of Sphinx and Sentinel Bay were under ice over the last 120 years, as glacial ice reached the lake shore in ~1200-1900 CE in both bays (Koch et al 2009). Rates of glacial retreat have been slightly higher for the Sphinx glacier than the Sentinel glacier in more recent years (1996-2003). In 1949, Sentinel Bay maintained a significantly larger area of glacial coverage in our study area, however the total amount of glacial retreat since the early 1900s has been roughly equal for the two sites (Koch et al 2009). The Sphinx and Sentinel glaciers are presently experiencing rapid retreat, and the newly exposed alpine surfaces provide a unique opportunity to follow successional changes in the region under global change.

Preliminary Data Acquisition

UAV imagery data was collected on July 30th and 31st, 2023 between 10 am and 6 pm in Sphinx Bay (solar noon 1:19 pm), and August 1st and 3rd between 10 am and 6 pm in Sentinel Bay (solar noon 1:18pm). Due to flight restrictions in the park, we were limited to two flight days within each bay. All flights were conducted using a DJI Mavic 3M drone and captured imagery both RGB (red, green, blue) and multispectral sensors. Band wavelengths for the multispectral sensor were 560 ± 16 nm for green (green-2), 650 ± 16 nm for red (red-2), 730 ± 16 nm for red edge (RE), and 860 ± 26 nm for near-infrared (NIR). The drones were flown at a height of 80-120 m above ground level (AGL) in areas with low slope and between 50-80 m AGL in higher elevation zones due to flight altitude restrictions. Ground reference points were placed on the site during drone flights to help georeference and align images into one large orthomosaic. All flights were flown in sunny conditions with low winds (< 20 kmph), with an average daily temperature between 18-20 ºC, and 65-70% relative humidity. The flight coverage areas represent the majority regions of interest for this study [defined in the introduction as deglaciated area] and is limited at the valley margins due to elevation and flight altitude. UAV flights covered areas of 0.926 km^2 for Sentinel Bay and 1.005 km^2 for Sphinx Bay respectively (Figure 1).

Ground-truthing data was obtained from a combination of presence-absence and relative abundance surveys of vegetation in the area (Table 1, Figure 2). Data was collected on August 1-3, 2023 at 42 sample locations, referred to as waypoints, across both glacial bays, with a minimum of 3 randomly selected locations within each of 4 major vegetation community types: Coniferous forest, deciduous forest (*Alnus viridis* dominated), deciduous shrub meadow (*Salix* spp. dominated) and wet meadow (*Equisetum* and *Juncus* spp. dominated). Survey teams sampled the presence and absence of species, and number of individuals of each species, in 1 x 1 m quadrat divided into 4 zones of 25 cm sections, recording the

© The Author(s) or their Institution(s)

presence/absence of species in each zone. The waypoint GPS coordinates were recorded at the central point of the quadrat using a Garmin GPS device. A dark diversity sampling scheme was also used, where the sampler walked in an outward direction from the waypoint, in a circular fashion creating a spiral shape. While doing this the surveyor recorded any observations of species that were not previously identified through the relative abundance sampling (i.e. quadrats) and then recording the distance from the individual of that species to the center of the quadrat using a 30 meter transect (Norton et al unpublished data 2025).

Of the 42 waypoints sampled, 30 had coniferous species present, 21 of which fell within the drone coverage area (11 for Sphinx Bay, 10 for Sentinel Bay) (Table 1, Figure 2a). Four coniferous species were identified in ground truthing data: *Tsuga mertensiana* (mountain hemlock), *Abies lasiocarpa* (subalpine fir), *Abies amabilis* (Pacific silver fir), and *Pinus albicalis* (whitebark pine). Only mountain hemlock (mhl) and subalpine fir (saf) were present within the quadrats, however, all species were identified using the spiralizing method. In total, 89 individuals were identified, with the vast majority being subalpine fir (49 individuals) and mountain hemlock (36 individuals). This led to 20 digitized tree polygons in Sphinx Bay: 9 mountain hemlock, 11 subalpine fir and 11 digitized tree polygons in Sentinel Bay: 5 mountain hemlock, 6 subalpine fir (Figure 2b- see *Imagery Preprocessing and Digitization of Conifers*). Pacific silver fir and Whitebark pine both each had two individuals identified, with only one of each in each bay. Because of the low amount of ground truthing data for *Pinus albicalis* and *Abies amabilis,* these species were excluded from further analyses and efforts were focused on *Tsuga mertensiana* (mountain hemlock) and *Abies lasiocarpa* (subalpine fir) given their prevalence in each site. The locations and details of all waypoints are listed in Table 1 and mapped in Figure 2.

Draft

© The Author(s) or their Institution(s)

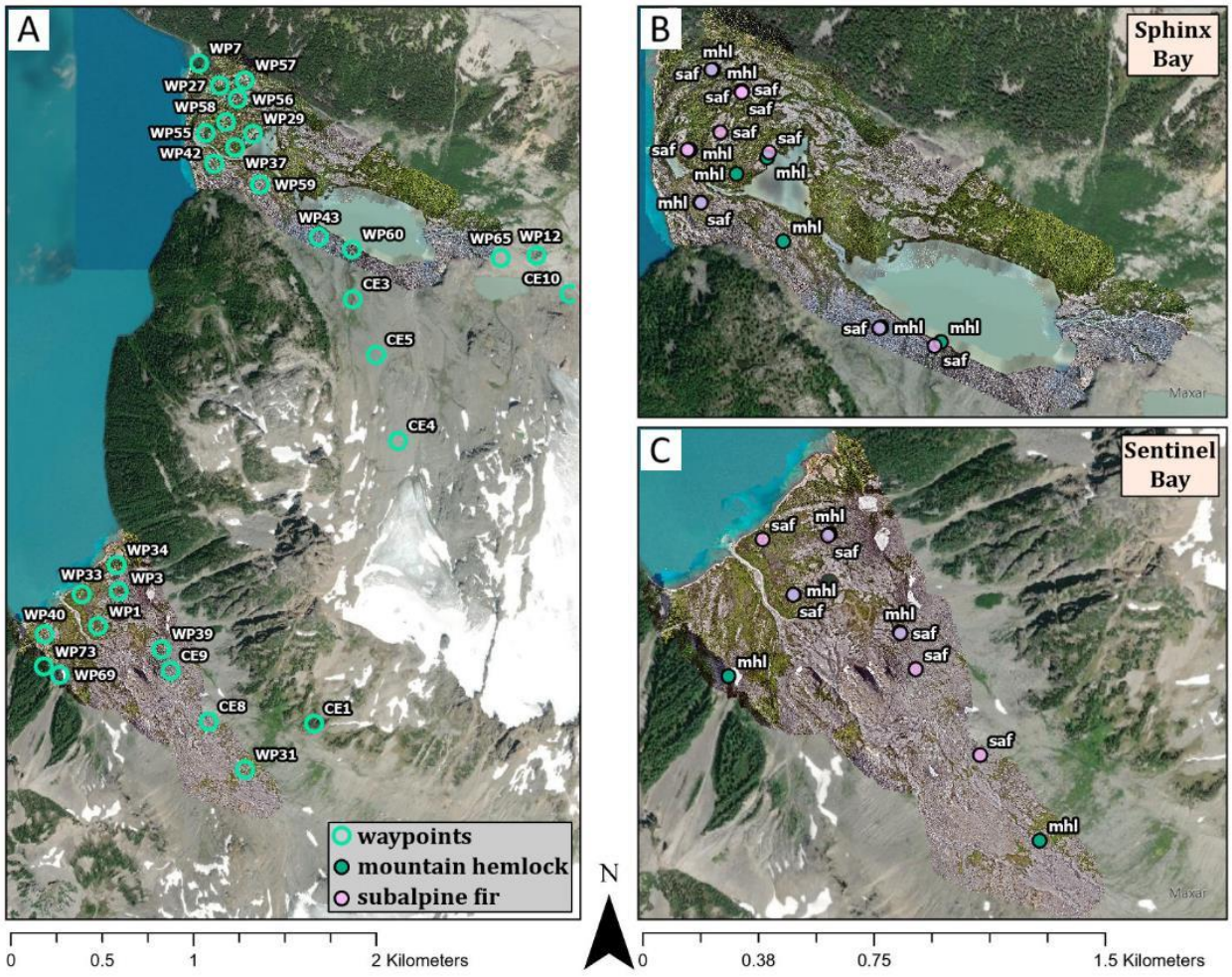


Figure 2: The locations of waypoints and trees in the guided dataset. Of 30 total waypoints, 21 overlapped with drone imagery, including 11 in Sphinx Bay and 10 in Sentinel Bay (A). From these waypoints, we identified 85 individual trees of our top 2 species of interest: subalpine fir (49 individuals- 32 in Sphinx and 17 in Sentinel) and mountain hemlock (36 individuals- 15 in Sphinx and 21 in Sentinel.) This led to 20 digitized tree polygons in B) Sphinx Bay: 9 mountain hemlock, 11 subalpine fir and 11 digitized tree polygons in C) Sentinel Bay: 5 mountain hemlock, 6 subalpine fir.

Table 1: Vegetation survey data used for the creation of training data. Of the 30 waypoints with conifers, 21 overlapped with the drone survey area, with 11 in Sphinx Bay and 10 in Sentinel Bay. From these waypoints, we identified 89 individual trees of our species of interest including 49 subalpine fir and 36 mountain hemlock. Spiral method denotes individual trees and their distance from the quadrats, while quadrats have 1-10 individuals per species each as indicated.

© The Author(s) or their Institution(s)

Name	Latitude, Longitude	CSRS UTM Zone 10N (easting, northing)	Spiral Method	Quadrats	Bay
WP43	49.92345, -122.98404	501146.7371, 5530119.067	saf, 9 m; mhl, 10 m; wbp, 39 m	-	Sphinx
WP58	49.92909, -122.99112	500638.4546, 5530746.055	saf, 5 m	-	Sphinx
WP42	49.92704, -122.99202	500573.8837, 5530518.123	saf, 4 m; mhl, 7 m	-	Sphinx
WP29	49.92851, -122.98906	500786.3152, 5530681.589	saf, 4 m; mhl, 20 m	-	Sphinx
WP55	49.92855, -122.99267	500527.2132, 5530686.005	mhl, 7 m	2 saf	Sphinx
WP27	49.93088, -122.99160	500603.9815, 5530945.069	mhl, 6 m	10 saf	Sphinx
WP56	49.93022, -122.99023	500702.3157, 5530871.7	mhl, 5 m	9 saf	Sphinx
WP60	49.92284, -122.98151	501328.3592, 5530051.287	mhl, 25 m	1 saf	Sphinx
WP37	49.92784, -122.99043	500687.9953, 5530607.083	mhl, 2 m; psf, 4 m	-	Sphinx
WP59	49.92602, -122.98853	500824.3975, 5530404.748	mhl, 19 m	-	Sphinx
WP57	49.93113, -122.98969	500741.0579, 5530972.882	-	6 mhl, 5 saf	Sphinx
WP31	49.89730, -122.98968	500742.2941, 5527211.565	saf, 7 m; mhl, 15 m	-	Sentinel
WP69	49.90196, -123.00379	499728.9454, 5527729.631	saf, 10 m	1 mhl	Sentinel
WP33	49.90591, -123.00213	499848.1669, 5528168.798	saf, 10 m	-	Sentinel
WP1	49.90435, -123.00089	499937.2054, 5527995.352	saf, 1 m; mhl, 2 m	-	Sentinel
WP73	49.90237, -123.00501	499641.3369, 5527775.221	psf, 1 m; wbp, 4 m	10 mhl, 8 saf	Sentinel
WP39	49.90321, -122.99604	500285.4865, 5527868.61	mhl, 3 m	1 saf	Sentinel
CE9	49.90216, -122.99535	500335.0432, 5527751.871	mhl, 16 m	1 saf	Sentinel
CE8	49.89966, -122.99245	500543.3272, 5527473.932	-	1 saf	Sentinel
WP3	49.90606, -122.99930	500051.3802, 5528185.474	mhl, 5 m	1 saf	Sentinel
WP40	49.90395, -123.00496	499644.9392, 5527950.89	-	4 mhl, 1 saf	Sentinel
CE10	49.92065, -122.96492	502519.3318, 5529808.222	saf, 7 m	-	Out of Bounds
WP7	49.93197, -122.99317	500491.2919, 5531066.248	saf, 1 m; psf, 8 m	2 mhl	Out of Bounds
WP12	49.92253, -122.96744	502338.3428, 5530017.164	psf, 4 m; mhl, 12 m	-	Out of Bounds
CE5	49.91766, -122.97968	501459.8761, 5529475.393	psf, 10 m	1 mhl	Out of Bounds
WP65	49.92242, -122.97017	502142.3824, 5530004.853	mhl, 18 m	-	Out of Bounds
CE1	49.89956, -122.98441	501120.7312, 5527462.903	-	1 saf	Out of Bounds
CE4	49.91344, -122.97800	501580.6201, 5529006.235	-	1 saf	Out of Bounds
WP34	49.90734, -122.99946	500039.8901, 5528327.788	-	1 mhl, 1 saf	Out of Bounds
CE3	49.92038, -122.98145	501332.7336, 5529778.89	-	3 mhl, 3 saf	Out of Bounds

174

175 ***Imagery Preprocessing and Digitization of Conifers***

176 UAV imagery was initially processed using Agisoft Metashape (Figure 3). To reduce file sizes
177 for computational efficiency, each bay was processed in four different sections. Images for each section
178 were processed into point clouds with coordinate precisions between 0.914 to 1.19 cm before being
179 processed into orthomosaics with a resolution of 1.83 to 2.38 cm per pixel and Digital Terrain Models

© The Author(s) or their Institution(s)

(DTMs) with a normalized resolution of 10 cm per pixel. Given a lack of reflectance targets in the imagery and sunshine sensor data retained for processing, the band values extracted were not calibrated for the influence of sunlight, instead being maintained as 16-bit DN values recorded by the sensor. Each orthomosiac and DTM raster produced by Agisoft Metashape was loaded into ArcGIS Pro and reprojected into CSRS UTM Zone 10N. This projection was chosen as the regionally appropriate variant for the standardized CSRS reference system for conducting surveys in Canada. Upon reprojection, each component raster of each bay was merged using the Mosaic to New Raster toolbox with a pixel type of 32 bit float, and a final resolution of 10 cm per pixel to match the resolution and extent of the DTMs (Figure 4). Units for the DTMs were set to elevation in meters and clipped to the same extent as its accompanying orthomosaic using the Clip Raster toolbox. Rasters for slope and aspect were constructed from each merged DTM using the Slope and Aspect toolboxes, respectively. Output measurements for slope raster generations were in degrees using a planar method, with the planar method used in aspect raster generations as well. Final multiband rasters for each glacial bay were produced using the Composite Bands toolbox using the orthomosaic (bands 1-7), the elevation (band 8), the slope (band 9), and the aspect (band 10) (Figures 5 and 6).

Four approaches to digitization of trees were attempted: two approaches of automated digitization using LiDAR360, and two approaches of manual digitization using photointerpretation. Prior to processing in LiDAR360, each point cloud was smoothed through a visual identification and manual removal of noise, with data found at higher elevations than was observed on site identified as noise. Ground points were generated, as were Digital Surface Models (DSMs), DTMs, and Canopy Height Models (CHMs). From the smoothed point clouds in LiDAR360, the Tree Segmentation tool was used to produce polygon shapefiles of trees. Segmentation by Point Cloud, and Segmentation by CHM were both attempted. Visual analysis of these outputs showed that these data had significant limitations for use in further analysis. The polygons defined as trees did not align consistently with the true location of trees or only covered a small portion of the treed areas without consideration for foliage coverage. Additionally, many polygons misrepresented boulders and other geological features in the bays as trees (Supplemental Figure S1). Thus, it was determined that automated digitization would not be as effective for the purposes of this study.

The two manual datasets of tree polygons were digitized using photointerpretation of the orthomosaic rasters in ArcGIS Pro. For both datasets, trees were digitized with an effort made to construct polygons which encompassed unshaded parts of each tree. The first dataset represents an attempt to manually relocate and identify the trees found in each waypoint of the ground-truthing vegetation survey, with each tree identified by species. For trees found within quadrats, polygons were constructed around

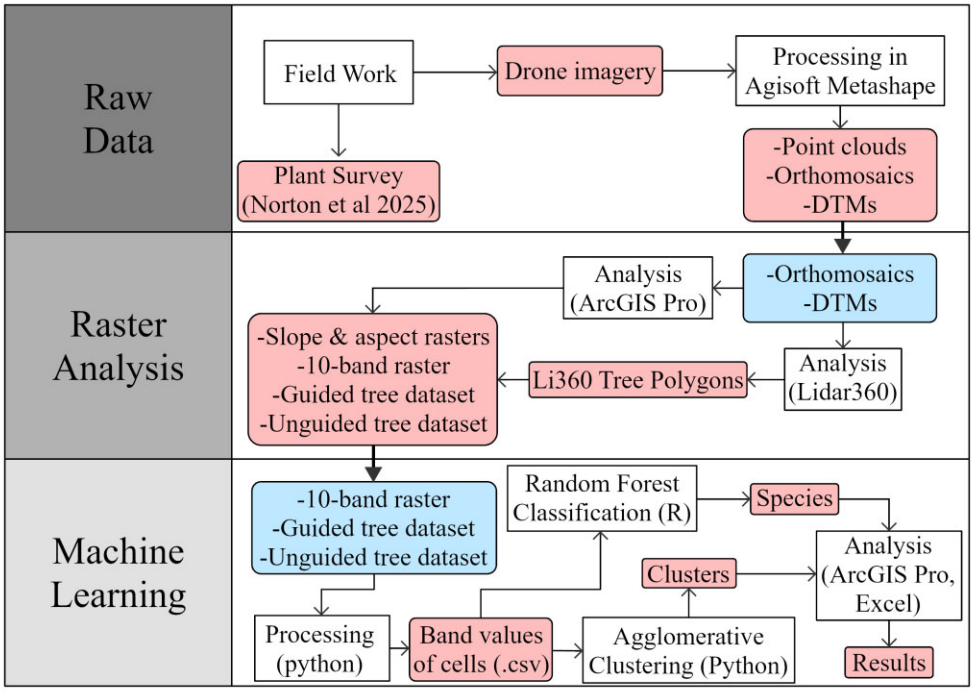
© The Author(s) or their Institution(s)

visibly vegetated cells in the zone of the quadrats indicated by the survey for each individual tree. For trees found using the spiralizing method, the distance recorded was used alongside the Measure tool in ArcGIS Pro to create a best guess for each tree identified. We used common morphological characteristics of each tree species (Subalpine fir- light blue-green, spire-like 'white' tip, cylindrical crown; Mountain hemlock- darker green, conical crown, wider spread branches) in combination with ground truthing data to draw polygons. Trees which were not clearly discernible were excluded. We refer to this dataset as the waypoint guided digitization, as it was created from the ground truthing waypoints. From the 89 individual trees, we created 31 total digitized tree polygons (as many polygons contained multiple individual trees): 11 subalpine fir and 9 mountain hemlock in Sphinx Bay and 6 subalpine fir and 5 mountain hemlock polygons in Sentinel Bay (Figures 2b & 2c) From these polygons, 6439 training points were generated in total, 2831 for subalpine fir and 3608 for mountain hemlock (see *Raster Cell Classifications)*.

The second digitization dataset represents a whole-area inspection. Only coniferous trees which were clearly discernible were included and polygons were manually drawn around crowns of individual trees. To limit computational load in areas of significant conifer coverage, we randomly digitized approximately half of the visible trees. This dataset includes 202 trees identified in Sphinx Bay and 236 trees identified in Sentinel Bay, with no guesses made on the species found. We refer to this dataset as the unguided digitization.

Draft

© The Author(s) or their Institution(s)



231

232 **Figure 3:** Workflow illustration beginning from raw data obtained by field work. Raw data was processed
233 primarily using Agisoft Metashape, with analysis primarily being completed in ArcGIS Pro. Machine
234 learning was completed with the programming languages Python and R. While some analysis was done
235 with LiDAR360, the outputs were not used for further analysis (see Supplemental Figure S1).

© The Author(s) or their Institution(s)

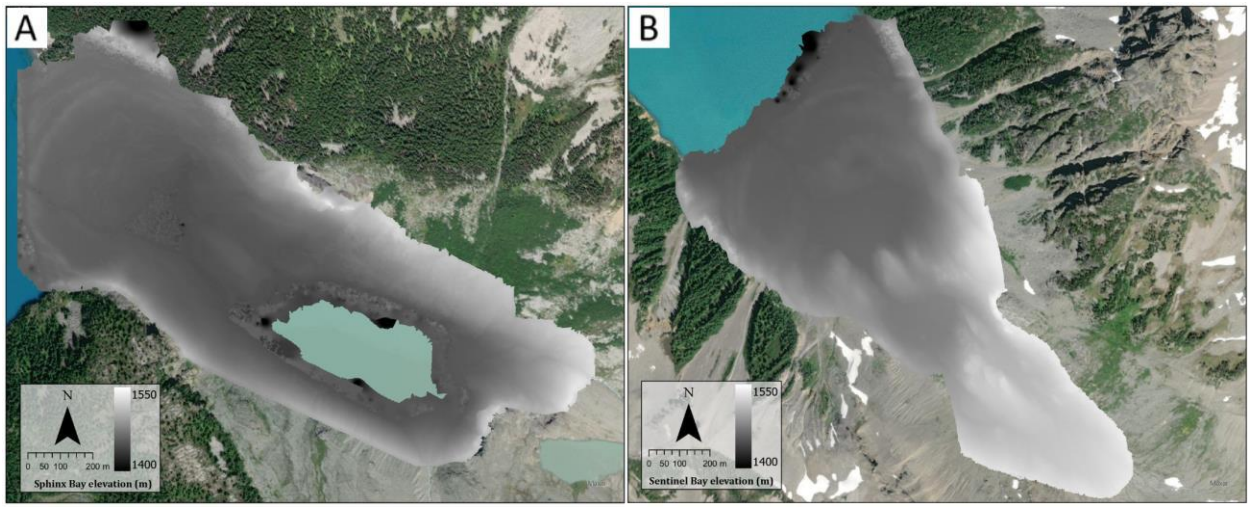


Figure 4: Digital Terrain Models for Sphinx (a) and Sentinel Bay (b). In Sphinx Bay, elevations quickly rise to 1460 m just past the shoreline of Garibaldi Lake before stabilizing and slightly decreasing, leading to a small lake of glacial outwash in the middle of the bay. Elevations tend not to exceed 1470 across most of Sphinx Bay but rise sharply to 1500 towards the back side of the bay approaching Sphinx glacier. In Sentinel Bay, elevations start at 1450 m at the shore of Garibaldi Lake and slowly rise until the middle of the bay where they quickly rise to 1500 m and above.

Draft

© The Author(s) or their Institution(s)

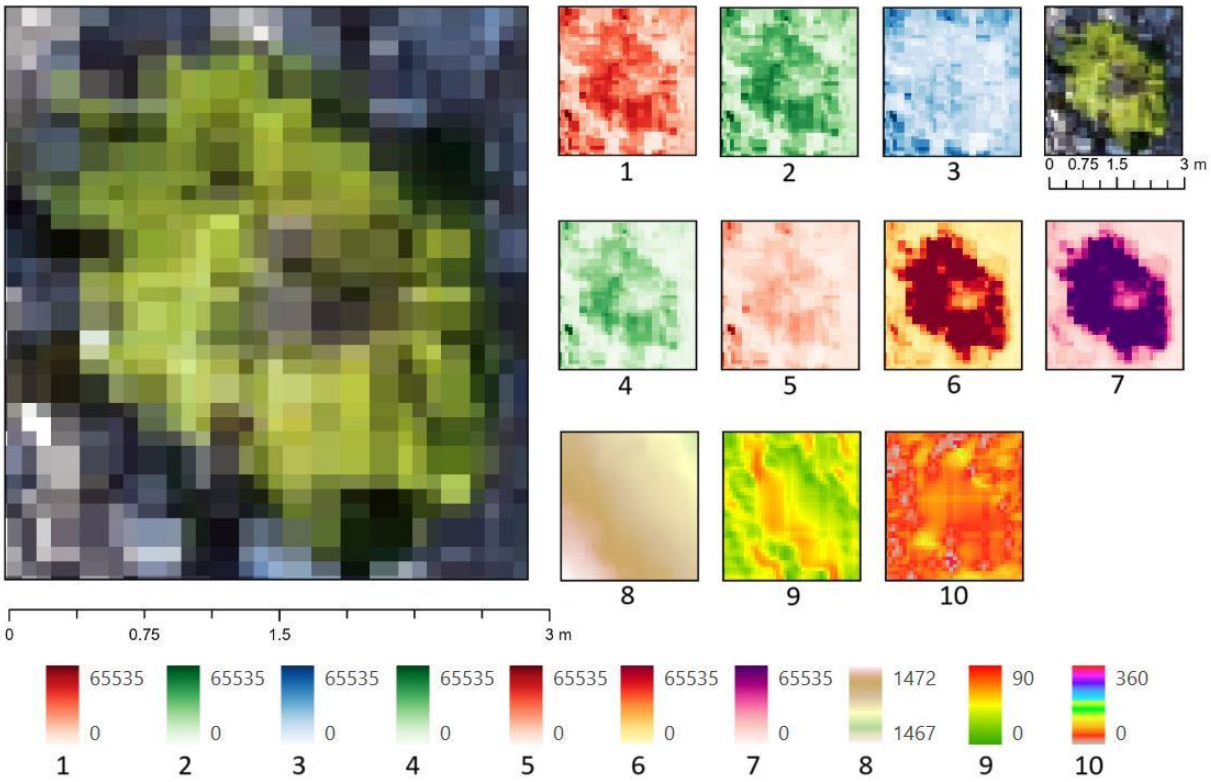


Figure 5: Drone-based RGB image of a mountain hemlock in Sphinx Bay with a resolution of 10 cm/px shown at left. Subpanels at right show the 10 bands captured with the multispectral camera with the numbers beneath each subpanel corresponding to the specific band values at a resolution of 10 cm/px: bands 1-3 represent red, green, and blue from the RGB camera. Bands 4-7 represent bands green-2, red-2, red-edge, and near-infrared from the multispectral camera. Bands 8, 9, and 10 represent the topographical characteristics of elevation (m), slope (%), and aspect (°) respectively. Both red-edge (6) and near-infrared (7) show strong contrast in the cells associated with foliage against the cells associated with terrain.

© The Author(s) or their Institution(s)

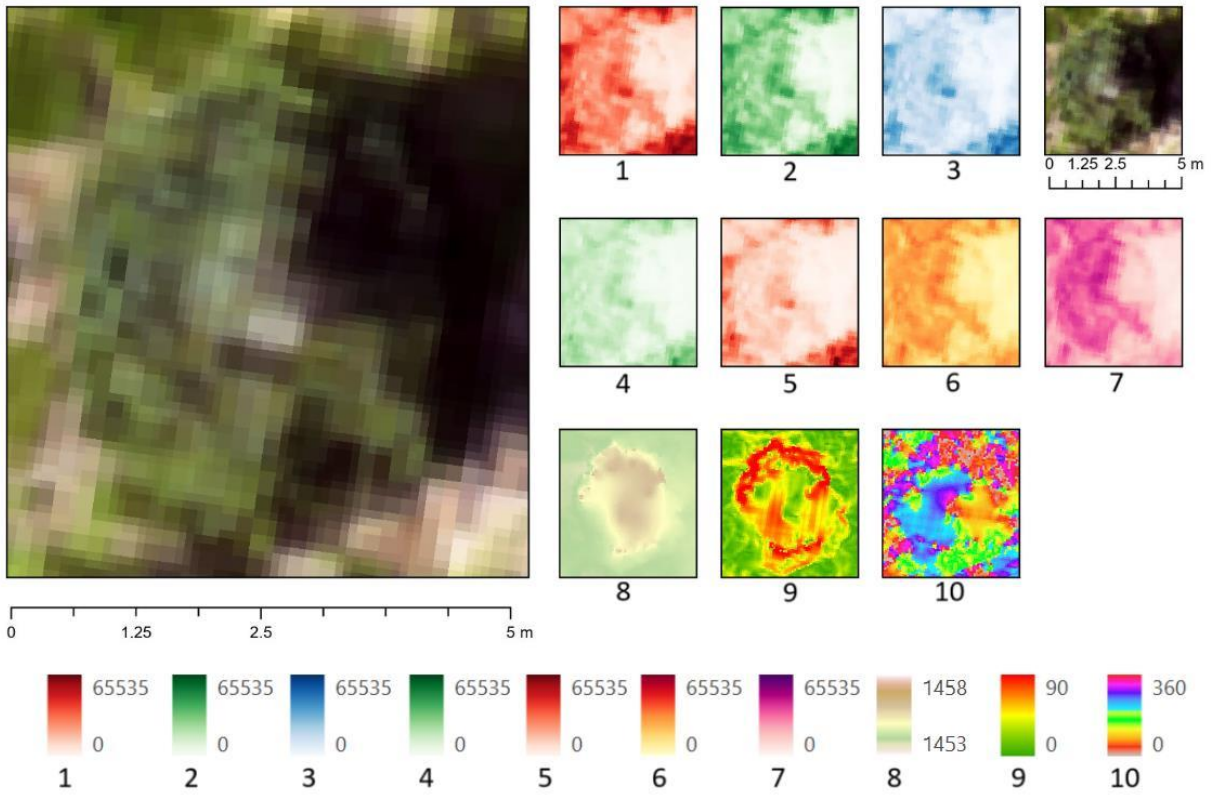


Figure 6: Drone-based RGB image of a subalpine fir in Sentinel Bay with a resolution of 10 cm/px shown at left. Subpanels at right show the 10 bands captured with the multispectral camera with the numbers beneath each subpanel corresponding to the specific band values at a resolution of 10 cm/px: bands 1-3 represent red, green, and blue from the RGB camera. Bands 4-7 represent bands green-2, red-2, red-edge, and near-infrared from the multispectral camera. Bands 8, 9, and 10 represent the topographical characteristics of elevation (m), slope, and aspect respectively. A clear increase in elevation (8) and slope (9) is visible beneath the subalpine fir, as well noticeably higher values for near-infrared (7) in the foliage as compared to the terrain.

Raster Cell Classifications

We first calculated the average and standard deviation of each raster band (1-10) for each species within each bay (Table 2). In the guided dataset, we sampled 100% of the raster cells overlapped by the tree polygons, leading to 6439 training points in total, 2831 for subalpine fir and 3608 for mountain hemlock. In the unguided dataset, we sampled 40% of the overlapped raster cells to stay within computational constraints. Next, two pixel-based machine learning approaches were used to classify the

© The Author(s) or their Institution(s)

cells of each raster within each polygon: an unsupervised agglomerative clustering and a supervised random forest classification (Figure 3). Each cell was recorded by a unique cell ID and associated polygon ID, allowing the majority classification of cells in each polygon to be determined, representing the prediction of species for each polygon.

The extraction of band values and the unsupervised agglomerative clustering classification were completed in python 3.12.7 using the libraries scikit-learn 1.5.2, rasterio 1.4.1, and geopandas 1.0.1. Prior to clustering, the data was standardized. We ran agglomerative clustering with default settings in scikit-learn with a range of cluster counts from 2-10, euclidean affinity, no connectivity, ward linkage, and compute_full_tree = False to find scenarios where clusters are associated with each target species (subalpine fir and mountain hemlock) based on species designations from the guided dataset. The supervised random forest classification was completed using the function 'ranger' in the ranger package in R (Wright & Ziegler 2017). We included all 10 bands as model inputs and ran 501 trees with an mtry = 3, permutation importance, a minimum node size =2 and split rule= "extra trees". We ran supervised classifications for each bay separately, with a 70-30 split on training and testing data respectively, and predictive accuracy was assessed through a confusion matrix of predictions on the test dataset. We assessed variable importance scores using the permutation method (Janitza et al 2015-) to determine which raster inputs were the strongest predictors of our species of interest in each bay. Finally, after training and testing the random forest classifier on the waypoint guided digitization, we then used the trained classifier to predict the species identity of individual tree polygons in the unguided digitization, with the same 10 raster bands as model inputs.

Draft

Table 2: Average band values within 1 standard deviation of conifers in the guided dataset. Significant overlap is present in the spectral bands, with most bands in both datasets having over 60% overlap. The overlap is greater in Sphinx Bay than in Sentinel Bay. The least overlap is seen in the blue band in Sentinel Bay, at 19.5%. Red-edge, near-infrared, elevation, and slope consistently exhibit less overlap than other band values.

Sentinel Guided Dataset

© The Author(s) or their Institution(s)

Band	Red	Green	Blue	Green-2	Red-2	Red-Edge	Near-Infrared	Elevation (m)	Slope (%)	Aspect (°)
subalpine fir	14038 - 24852	17053 - 28534	9913 - 19633	8569 - 14097	4164 - 7919	16216 - 27302	18230 - 29962	1444 - 1474	19 - 60	119 - 286
mountain hemlock	15808 - 22759	19352 - 27149	7435 - 12291	8620 - 13559	3479 - 5421	20800 - 31536	21872 - 34247	1452 - 1507	4 - 36	111 - 303
overlap	15808 - 22759	19352 - 27149	9913 - 12291	8620 - 13559	4164 - 5421	20800 - 27302	21872 - 29962	1452 - 1474	19 - 36	119-286
overlap (%)	64.3	67.9	19.5	89.3	28.3	42.4	50.5	34.9	30.4	119-286
Sphinx Guided Dataset										
Band	**Red**	**Green**	**Blue**	**Green-2**	**Red-2**	**Red-Edge**	**Near-Infrared**	**Elevation (m)**	**Slope (%)**	**Aspect (°)**
subalpine fir	10871 - 25255	14132 - 29245	6593 - 15859	7180 - 14205	3217 - 6446	15967 - 33596	15692 - 35110	1455 - 1464	8 - 26	62 - 298
mountain hemlock	12947 - 26123	15704 - 29044	7569 - 18403	7777 - 14263	3527 - 6824	18888 - 41705	20723 - 46021	1451 - 1460	17 - 42	54 - 287
overlap	12947 - 25255	15704 - 29044	7569 - 15859	7777 - 14205	3527 - 6446	18888 - 33596	20723 - 35110	1455 - 1460	17 - 26	62 - 287
overlap (%)	80.7	88.3	70.2	90.8	80.9	57.1	47.4	38.5	26.5	92.2

Results

Out of 85 trees observed by the ground-truthing waypoint data, 36 were identified as likely mountain hemlock and 49 were identified as likely subalpine fir. Sphinx Bay had a higher proportion of subalpine fir than mountain hemlock, with 32 and 15 individuals, respectively. Sentinel Bay had a more even spread with 17 subalpine fir and 21 mountain hemlock. Many trees in the dataset came in pairs wherein both target species were found in quadrat plots near the waypoint, reducing the potential for spatial comparison of each species or cluster group in this dataset (Table 1).

The random forest classification showed high accuracy (98% and 99% for Sphinx, Sentinel Bay respectively) in its predictions onto the held-out portion (i.e. 30%) of the training dataset. Out of 919 held-out training points in Sentinel Bay, the model correctly predicted the species identity for 293, 618 points and incorrectly for 3, 5 points for mountain hemlock and subalpine fir respectively. Similarly in Sphinx Bay, out of 1012 held-out training points, the model correctly predicted the species identity for 754, 235 points and incorrectly for 18, 5 points for mountain hemlock and subalpine fir respectively (Figure 7).

After training and testing, the random forest model predicted species classifications onto the unguided dataset. At the polygon-scale, of 202 individual tree polygons in Sphinx, 193 had a majority of their cells classified as mountain hemlock while 9 had a majority classified as subalpine fir. In Sentinel, 236 individual tree polygons were composed of 24 with a majority cells predicted mountain hemlock and

© The Author(s) or their Institution(s)

212 with a majority cells predicted subalpine fir. In Sphinx Bay, the limited subalpine fir were primarily found in the northern half of the site, with 6 found within a 30 meter radius of each other in the northeastern corner. Mountain hemlock trees were spread throughout the bay, but had a similar tendency to primarily be found in stands of species-grouped trees. In Sentinel Bay, all trees were found within the first kilometer from the shoreline with Garibaldi Lake, with 220 found within 500 meters of the shoreline (Figure 8). Subalpine fir exhibited a clumped distribution pattern, particularly near the lake, while mountain hemlock exhibited no clear distribution patterns.

Elevation was the strongest predictor of species classification within each bay based on permutational variable importance (Table 3). In the guided dataset, the mean elevation of mountain hemlock and subalpine fir in Sphinx Bay were 1455.8 and 1460.0 meters respectively. In Sentinel Bay, the mean elevation values were 1480.2 and 1459.6 meters. In the unguided dataset, for mountain hemlock and subalpine fir respectively, the mean elevations were 1466.9 and 1485.0 meters for Sphinx Bay, and 1462.9 and 1460.9 meters for Sentinel Bay. The second strongest predictors for each bay were based on spectral information i.e. the near-infrared band for Sphinx Bay and the Blue band for Sentinel Bay. Of the multispectral bands, the red-edge and near-infrared bands represented the bands with the least overlap (within 1 standard deviation) between species in Sphinx (Table 2, S1), while the blue and red-multispectral bands represented the least overlap between species in Sentinel (Table 2, S1). The third and fourth strongest predictors of species classification in Sphinx Bay were topographic (Aspect, slope) while at Sentinel Bay they were multispectral (red-edge, red multispectral).

Agglomerative clustering outputs with 3 and 6 clusters produced the most meaningful data of all cluster counts. When compared to the guided dataset, for Sentinel Bay, both 5 and 6 clusters resulted in a strong association of 0 to subalpine fir, with 877 of 883 cells classified as cluster 0 coming from subalpine fir cells in the 5-cluster scenario, and all 635 cells classified as cluster 0 coming from subalpine fir cells in the 6-cluster scenario (Figure 9). Additionally, cells classified as cluster 5 (n=248) were distributed with 6 being assigned to mountain hemlock cells, while the other 242 were assigned to subalpine fir cells. A majority association to mountain hemlock was found in cluster group 2 in all datasets, and in cluster group 1 in the 5 and 6-cluster scenarios. No dataset resulted in a strong association for mountain hemlock cells for Sentinel Bay, with the strongest being cluster 2 for each dataset (n=503) at 73.4 percent. For Sphinx Bay, a high association of cluster 2 to mountain hemlock was found in each dataset, with each dataset having 12 subalpine fir cells and 324 mountain hemlock cells (Figure 10). No dataset resulted in a strong association for subalpine fir cells in Sphinx Bay, with the strongest being clusters 4 in the 5-cluster dataset and cluster 1 in the 6-cluster dataset at 42.3% each, with both having 308 of 728 cells classified as subalpine fir.

© The Author(s) or their Institution(s)

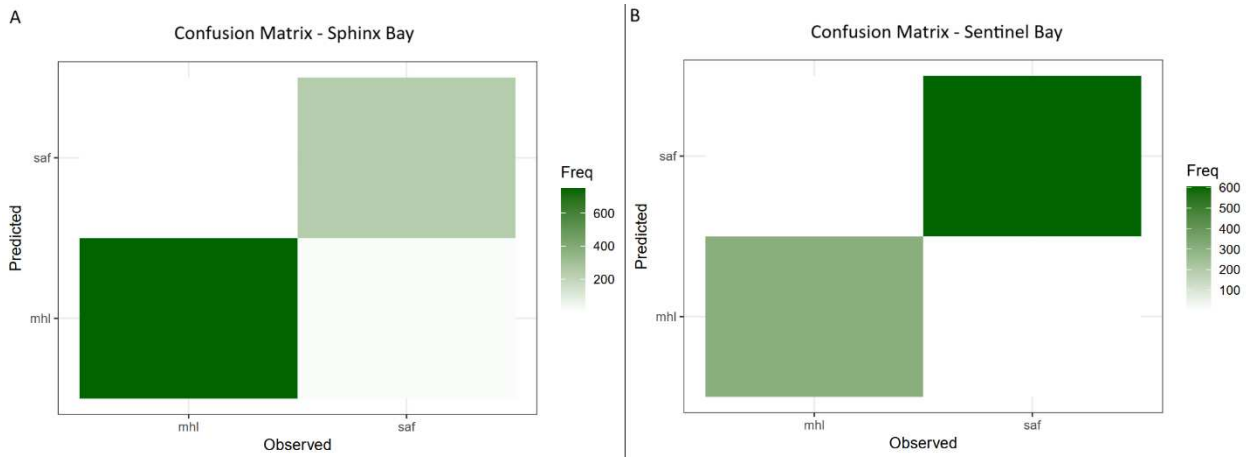


Figure 7: Accuracy of Random Forest predictions onto held-out portions of the training dataset (30%) for each species in each bay. The trained classifier predicted known species identities with 99% accuracy in Sentinel Bay and 98% accuracy in Sphinx Bay respectively.

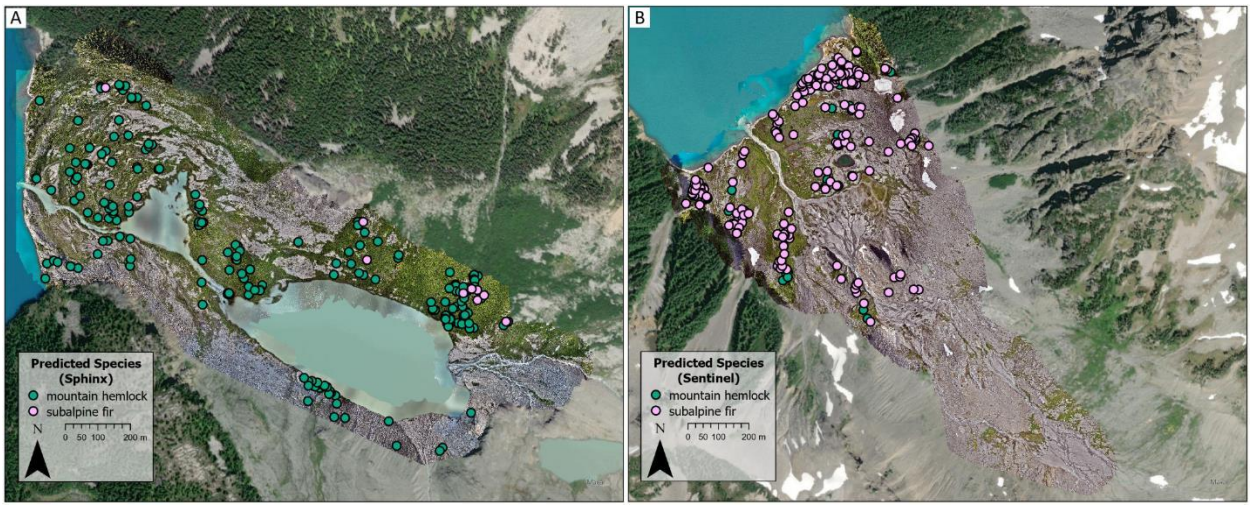


Figure 8: Random Forest predictions of each species in each bay across the unguided digitization dataset. Sphinx Bay exhibits a predominance towards mountain hemlock and a distribution throughout the bay. Sentinel Bay exhibits a predominance towards subalpine fir with a majority found closer to Garibaldi Lake in a clumped distribution.

© The Author(s) or their Institution(s)

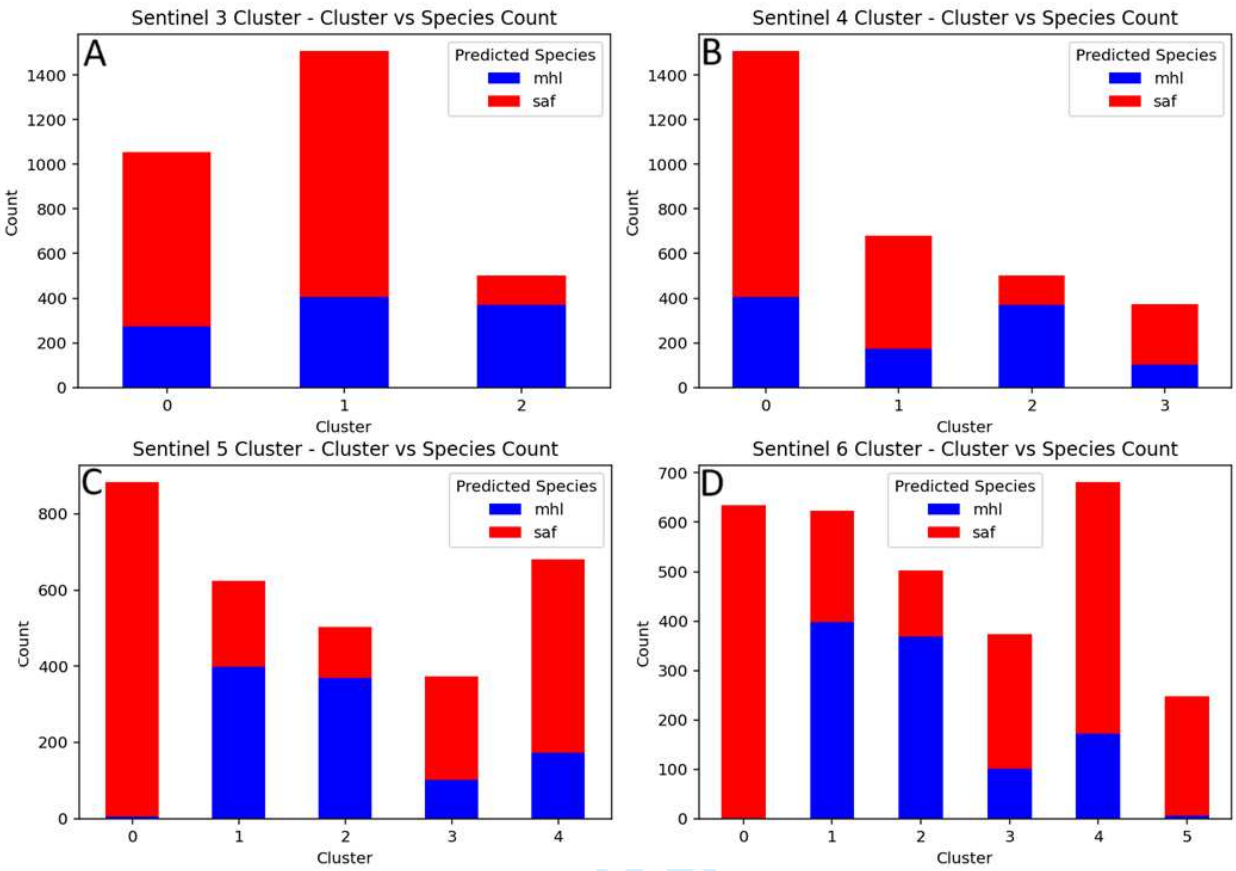


Figure 9: Comparison of cluster group assignments to species of cells in the guided dataset in Sentinel Bay for 3 to 6-cluster datasets. A strong association of cluster group 0 to subalpine fir is found in 5 and 6-cluster datasets, and of cluster group 5 in the 6-cluster dataset. The majority of associations to mountain hemlock are found cluster 2 in all datasets, and in cluster 1 in the 5 and 6-cluster datasets. No strong associations for mountain hemlock are found.

© The Author(s) or their Institution(s)

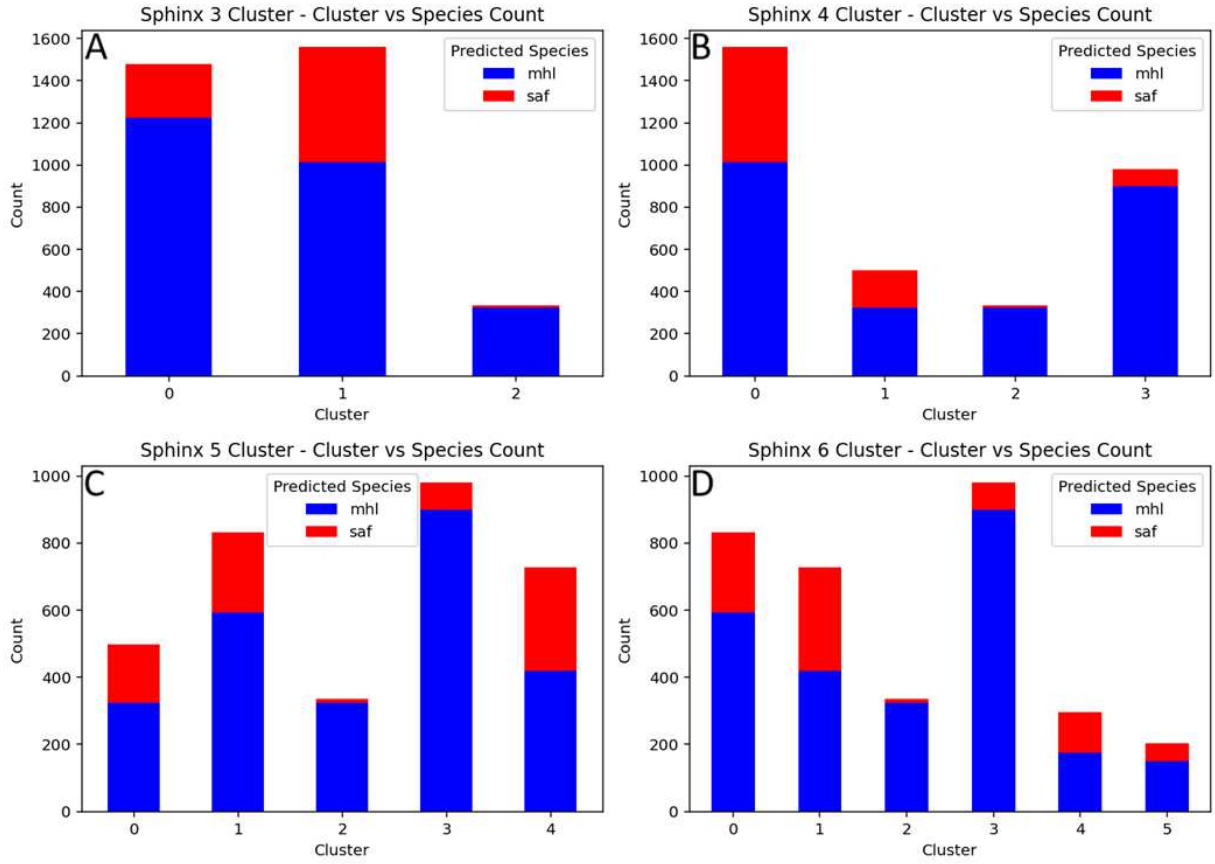


Figure 10: Comparison of cluster groups assignments to species of cells in the guided dataset in Sphinx Bay for 3 to 6 cluster groups. A strong association of cluster group 2 to mountain hemlock is found in all datasets, but no other strong associations are found.

Table 3: Permutational variable importance values from the random forest classification for all 10 raster layers across both bays. Variables are listed from most important (highest values) to least important (lowest values) within each bay.

Bay	Variable	Variable Importance
Sphinx	Elevation	0.189
	Near-infrared (NIR)	0.087

© The Author(s) or their Institution(s)

	Slope	0.073
	Aspect	0.073
	Red multispectral	0.051
	Blue	0.048
	Red-edge (RE)	0.044
	Green multispectral	0.040
	Red	0.039
	Green	0.037
Sentinel	Elevation	0.226
	Blue	0.108
	Red-edge (RE)	0.068
	Red multispectral	0.062
	Near-infrared (NIR)	0.060
	Slope	0.041
	Green	0.035
	Red	0.031
	Green multispectral	0.029
	Aspect	0.014

Draft

Discussion

Developing climate change outlooks for tree species across British Columbia is a key research objective of government agencies, academic institutions and the larger forest industry today (BC Ministry of Forests 2012, metro Vancouver 2017). Subalpine fir and Mountain hemlock are core species of subalpine forests across the province, with Subalpine fir being the second most widely distributed species in BC (Bunnell & Kremsater 2012). Subalpine fir is known to establish after fire in mountains of the Pacific Northwest, highlighting its ability to recolonize highly disturbed areas (Little et al 1994). While many climate change predictions have suggested that the ranges of these species will decline with warmer temperatures (Green 2005, LLoyd & Bunn, Bunnell & Kremsater 2012) the potential for infilling of these species into recently deglaciated areas has not been considered (to our knowledge) in these projections. Our findings suggest that subalpine fir may be more well suited for inital infilling into postglacial areas, followed by Mountain Hemlock, however, the timeline of soil development will be a key limiting factor in these considerations (Peterson & 2001, Peterson et al. 2002)

© The Author(s) or their Institution(s)

Our study predicted a strong spatial-dependence of species occurrence with a majority of subalpine fir in Sentinel Bay and a majority of mountain hemlock in Sphinx Bay. This likely is influenced by the differences in the glacial histories and environmental conditions of each bay. Exposure to sunlight may be of particular importance as Sentinel Bay is south of Garibaldi Lake, with direct sun exposure coming from the north to northwest. By contrast, Sphinx Bay is located east of the lake with direct sun exposure coming mostly from the west to northwest. Consequently, Sentinel Bay is more shielded from sun exposure than Sphinx Bay and receives significantly less incoming solar radiation (Figure 11), contributing to a longer lasting snowpack and more poorly developed soils. On the other hand, Sphinx Bay receives more direct sunlight, particularly strong afternoon sun due to its west facing aspect and has more highly developed soils, supporting greater overall vegetation cover (Figure 8). Overall, the greater sun exposure in Sphinx Bay contributes to environmental conditions consistent with more rapid successional trajectories post deglaciation and higher temperatures in contrast with Sentinel Bay, which has conditions more similar to true tundra or alpine environments. Previous research has found that subalpine fir has a root cold hardiness of -11.5 degrees C as compared to –7.5 ºC for mountain hemlock (Coleman 1992), suggesting that subalpine fir may more readily establish in colder environments than mountain hemlock. Subalpine fir may exhibit a negative correlation to increase in temperature and higher soil water availability from corresponding glacial melt, which is a limiting factor for subalpine fir growth (Haghshenas & Wood 2024), (Peterson et al 2002). At these higher temperatures and more mesic soil conditions, subalpine fir may then be outcompeted by mountain hemlock (Brunnel & Kremsater 2012), consistent with the differences in spatial trajectories observed across the two bays.

Subalpine fir has also been found to exhibit more clumped distribution patterns due to layering (Uchytil 1991, Astrup et al 2008, Nitschke 2012). In recently deglaciated landscapes, soil moisture will be highest nearer the glacier and will diminish with distance from the glacier (Strauss et al 2009), provided no new water sources enter the system. This suggests that more recent glaciation may have been an influencing factor in the predominance of subalpine fir clumps in Sentinel Bay, with less recent glacial retreat and more recent glacial advance as compared to Sphinx Bay (Koch et al 2009). These findings suggest that subalpine fir and mountain hemlock may follow distinct postglacial successional patterns, with subalpine fir being more tolerant of poorly developed paraglacial soils and mountain hemlock preferring more well-developed mesic soils (Brunnel & Kremsater 2012). While mountain hemlock also tolerates low temperatures and exhibits sensitivity to moisture availability (Peterson & Peterson 2001), mountain hemlock exhibits high prevalence in later successional stages of deglaciated landscapes, likely due to its requirements for more well-developed soil profiles (Klaar et al 2014). This successional pattern from subalpine fir to mountain hemlock has been described in previous studies (Petterson et al. 2002), but not in the context of contemporary deglaciation.

© The Author(s) or their Institution(s)

Both conifer species exhibited significant overlap in their band values, which would be expected given the similarities in foliage traits among conifer species. Previous research attempting to find spectral band values of foliage in forests has found high accuracy in deciduous forests during senescence, which would capture greater variation in multispectral band values (Schiefer et al 2020, Jiang et al 2023). The decreased percentage of overlap between the two species in elevation, near infrared, and blue values suggest the potential to derive differences among species based on a combination of spectral and geomorphic information. In particular, the high variable importance of elevation in both bays suggests species specific preferences in growing conditions, aligning with previous literature highlighting the importance of topographic niches in mapping species in alpine environments (Dirnböck 2003). Identification and mapping of geomorphic drivers may be of particular importance in understanding succession patterns in paraglacial landscapes (Klaar et al 2014), (Ramskogler et al 2023). Accuracy and confidence in results in classifying coniferous species can further be improved using object-based classification (Duro et al 2012, Franklin 2018). Object-based classification, as compared to pixel-based classification, has been found to be more accurate in both coniferous and deciduous forests, resulting in a higher accuracy of species predictions in coniferous forests (Franklin et al 2017, Franklin 2018), as well as in other land-cover classifications (Duro et al 2012).

In this study, the ability of agglomerative clustering to identify cluster groups which correlated highly with species designations in cells suggests the potential for unsupervised classifications to provide initial insights into species groups, mirroring its potential for initial examinations in existing literature (Franklin 2018). While agglomerative clustering can provide some insight into species designations without having immediate access to ground truthing or other applicable training data for supervised classification, further work must be done to identify which bands of information provide the most detail in identifying species-specific differences between trees. Likewise, work must be done to identify which cluster groups denoted species-level groupings as opposed to other tree characteristics such as health or age.

The data and analysis had limitations in the preliminary data availability and in the consistency of the drone imagery. Given that the ground truthing data required further effort to try to identify the specimens which were observed in the field in the accompanying drone imagery, there is a chance for error through misattribution of species designations. Likewise, the field surveys did not completely align with the drone surveys as a substantial portion of the ground truthing data was found outside the areas of drone coverage. Furthermore, much of the ground survey data found within the bays was not usable as training data due either to species being indistinguishable, particularly within quadrat datasets which contained both species, or the presence of other species in the dataset which were not used for this

© The Author(s) or their Institution(s)

analysis. When compounded with the potential for interpretative error during a visual interpretation of the drone imagery, this greatly limited the quantity and quality of training data that could be fed into the random forest classification. The visual interpretative error also provides potential bias to arise when observing trees in the drone imagery itself, without the help of waypoints, as trees identified by waypoints set the standard of what to look for. A bias towards subalpine fir was possible due to the clear spire form and grayish-white center.

Additional limitations are present in the timing and consistency of the drone imagery. The drone imagery was limited by regulations of the park which only allowed for a short window of flying time (2 days). Because of this, the drone imagery includes a variety of shadows cast from trees which imply changes in the time of day when flights were completed. The angle of light at the time of capture can affect the band values in foliage. The 8-hour window of the flights can result in significant differences in the light angles observed at this site. Previous research has attempted to control for solar reflectance, which can have a significant impact on the results obtained from remote sensing data (Jiang et al 2023). It is assumed for this study that the variability found within foliage samples can represent a range of values obtained despite solar reflectance for each species. Despite these challenges, random forest classification was able to achieve relatively high accuracy for species distinctions with a combination of spectral and geomorphic variables from the drone imagery, and variable importance identified high predictive power of the NIR bands for species distinctions in line with other research (Donnini et al 2024, Vaillant et al 2024).

Suggestions for future research include increased ground truthing data with accompanying markers for clear identification in orthoimagery, inclusion of additional samples of less common species (e.g. Abies amabilis (Pacific silver fir), and Pinus albicalis (whitebark pine)), more controlled timing of drone flights and incorporation of sunlight sensor data, further investigations into the use of agglomerative clustering or other deep learning techniques such as convolutional neural networks (CNNs) (Schiefer et al 2020) to identify species-specific differences without ground-truthing data, and the use of object-based classification in tandem with pixel-based classification. At this site in particular, comparative assessments of the vegetation communities in each bay in the future could assess what roles deglaciation timing and sun exposure have in successional dynamics at the landscape scale.

Conclusions

© The Author(s) or their Institution(s)

The overarching goal of this research was to improve our understanding of, and ability to predict, forest succession in post glacial areas, which is a landscape level impact of climate change in BC that is currently understudied. Current climate predictions for forest ecosystems primarily focus on changes to the forested land base, and this research fills an important knowledge gap for how historically non-forested areas will change into the future. Furthermore, defining multispectral signatures for key BC tree species is an important methodological development for UAV imagery processing which can be applied in other forestry applications such as geospatial tree inventories. By incorporating specific-specific information, this extension can greatly improve the accuracy of estimates for productivity or carbon storage at the landscape level. Finally, the use of drone imagery in research also provides the added benefit of improving communication with stakeholders and adequately conveying landscape level changes through visuals and mapping (Sakals 2019).

Draft

© The Author(s) or their Institution(s)

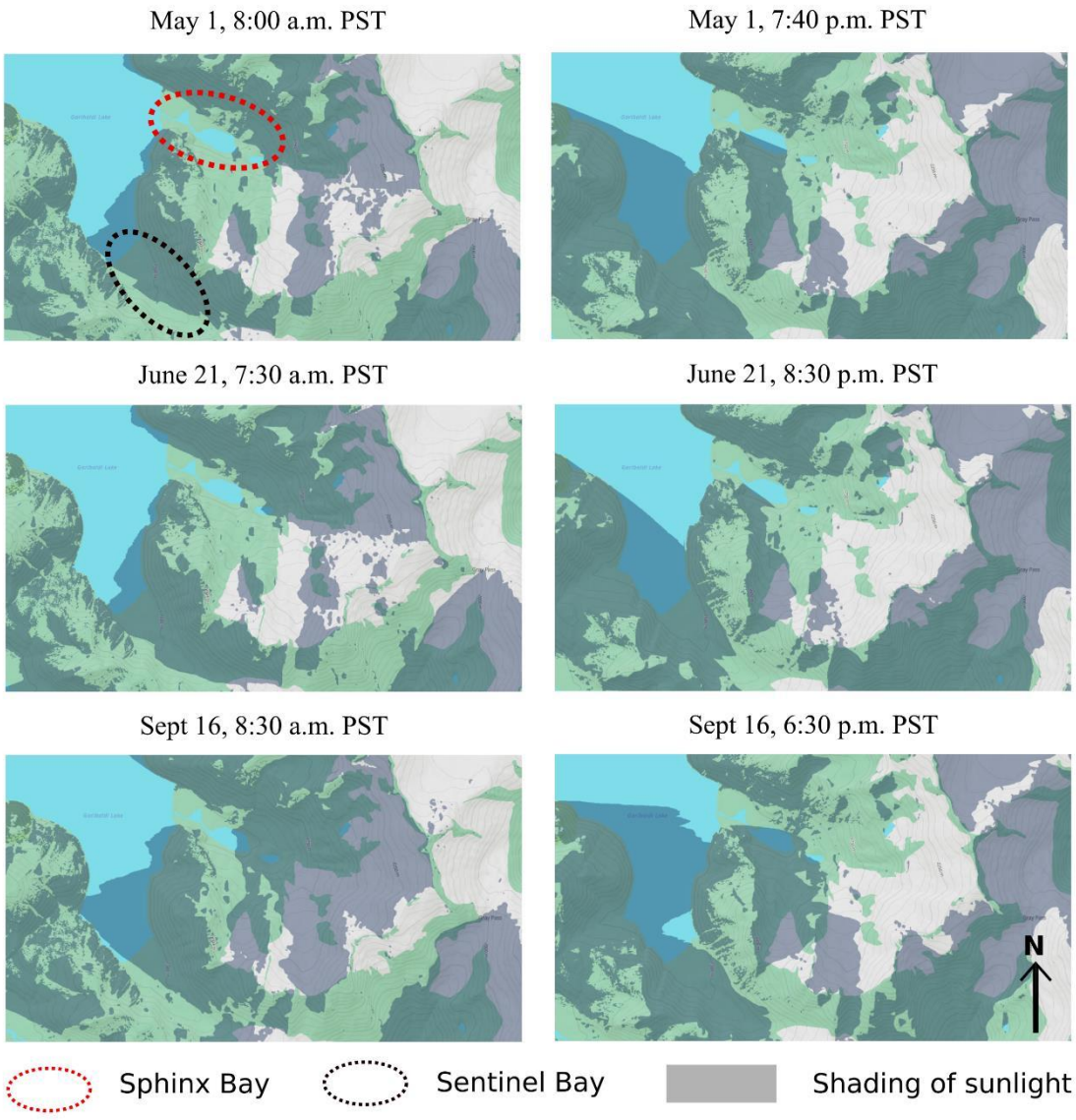


Figure 11: Sun exposure to each bay in the morning and evening on May 1, June 21, and Sept 16. Sentinel Bay experiences shading from the surrounding topography for 1-3 more hours daily than Sphinx Bay. At all 6 sampled times, Sentinel Bay is mostly or completely shaded while Sphinx Bay is mostly or completely exposed. Sun exposure maps created using the only tool "ShadeMap.app (https://shademap.app)".

Acknowledgements

© The Author(s) or their Institution(s)

We acknowledge that this research was conducted on the lands of the Skwxwú7mesh (Squamish), Lil'wat and Sḵwx̱wú7mesh peoples. Studying the biodiversity of this region would not be possible without their past, present and future stewardship. Nch'k̲ay̓ is the Skwxwú7mesh name for the mountain of which Garibaldi Provincial Park is named, which translates to "dirty water" or "grimy one," in reference to the volcanic dust from this stratovolcano (Squamish Nation 2023, BC Geographical Names). We are grateful to BC Parks for providing permissions to conduct research in the Park including the drone and ground truthing surveys. We thank the undergraduate research assistants and volunteers for their contributions to the ground vegetation survey and transport of equipment for the drone surveys.

Competing Interests

The authors declare that they have no competing interests.

Consent for Publication

As per the Ministry of Forests (FOR) Research Program, this document has undergone the required scientific peer review for the publication format, document type, and topic and has had a management implications review. Manager's approval for publication has been provided and documented.

Funding

Funding for this study was provided by the Ministry of Forests – Province of British Columbia, and BC Parks Living Labs for Climate Change and Conservation Program.

Availability of Data and Materials

Processed data and analysis scripts can be found at https://figshare.com/s/42ddfd251ebdb2ff551d. Following peer review if the manuscript is accepted for publication the repository will be made public.

Authors' Contributions

EA contributed to the final processing of drone data and drafted the manuscript. CGC developed the study, secured the funding, collected field drone and ground truthing data, participated in data analysis and supported preparation of the manuscript. SMC participated in data analysis and supported preparation of the manuscript. SY collected field drone data and assisted with initial data analysis. CN and CE developed the ground truthing survey protocol and collected and processed all ground truthing data.

References

Agee, J.K. and Smith, L. (1984) 'Subalpine Tree Reestablishment After Fire in the Olympic Mountains, Washington', *Ecology*, 65(3), pp. 810–819. Available at: https://doi.org/10.2307/1938054.

© The Author(s) or their Institution(s)

Draft

Astrup, R., Coates, K.D. and Hall, E. (2008) 'Recruitment limitation in forests: Lessons from an unprecedented mountain pine beetle epidemic', *Forest Ecology and Management*, 256(10), pp. 1743–1750. Available at: https://doi.org/https://doi.org/10.1016/j.foreco.2008.07.025.

Baron, J.N. *et al* (2024) 'Fuel types misrepresent forest structure and composition in interior British Columbia: a way forward', *Fire Ecology*, 20(1), p. 15. Available at: https://doi.org/10.1186/s42408-024-00249-z.

BC Geographical Names Office (2023) [Nch'k̲a̓y̓] Information provided by Squamish Nation. BC Geographical Names. Available at: https://apps.gov.bc.ca/pub/bcgnws/names/74958.html (Accessed: 27 May 2025)

Beedle, M.J., Menounos, B. and Wheate, R. (2015) 'Glacier change in the Cariboo Mountains, British Columbia, Canada (1952–2005)', *The Cryosphere*, 9(1), pp. 65–80. Available at: https://doi.org/10.5194/tc-9-65-2015.

Brink, V.C. (1959) 'A Directional Change in the Subalpine Forest-Heath Ecotone in Garibaldi Park, British Columbia', *Ecology*, 40(1), pp. 10–16. Available at: https://doi.org/10.2307/1929917

Bunnell, F.L. and Kremsater, L.L. (2012) 'Migrating like a Herd of Cats: Climate Change and Emerging Forests in British Columbia', *Journal of Ecosystems and Management*, 13(2), pp. 1-24. Available at: https://doi.org/10.22230/jem.2012v13n2a131

Coleman, M.D. et al. (1992) 'Root cold hardiness and native distribution of subalpine conifers', *Canadian Journal of Forest Research*, 22(7), pp. 932–938. Available at: https://doi.org/10.1139/x92-124.

Danby, R.K. And Hik, D.S. (2007) 'Variability, contingency and rapid change in recent subarctic alpine tree line dynamics', *Journal of Ecology*, 95(2), pp. 352–363. Available at: https://doi.org/https://doi.org/10.1111/j.1365-2745.2006.01200.x.

Dirnböck, T. et al. (2003) 'Mapping alpine vegetation based on image analysis, topographic variables and Canonical Correspondence Analysis', *Applied Vegetation Science*, 6(1), pp. 85–96. Available at: https://doi.org/https://doi.org/10.1111/j.1654-109X.2003.tb00567.x.

Donnini, J., Kross ,Angela and and Alejo, C. (2024) 'Spectral Diversity as a Predictor of Tree Diversity: Exploring Challenges and Opportunities Across Forest Ecosystems', *Canadian Journal of Remote Sensing*, 50(1), p. 2403495. Available at: https://doi.org/10.1080/07038992.2024.2403495.

Duro, D.C., Franklin, S.E. and Dubé, M.G. (2012) 'A comparison of pixel-based and object-based image analysis with selected machine learning algorithms for the classification of agricultural landscapes using SPOT-5 HRG imagery', *Remote Sensing of Environment*, 118, pp. 259–272. Available at: https://doi.org/https://doi.org/10.1016/j.rse.2011.11.020.

Eichel, J., Stoffel, M. and Wipf, S. (2023) 'Go or grow? Feedbacks between moving slopes and shifting plants in high mountain environments', *Progress in Physical Geography*, 47(6), pp. 967–985. Available at: https://doi.org/10.1177/03091333231193844.

© The Author(s) or their Institution(s)

Erica, C. et al. (2024) 'Glacier Retreat Effects On Ecosystem Development And Carbon Dynamics', *bioRxiv* [Preprint]. Available at: https://doi.org/10.1101/2024.10.06.616884.

Fell, S.C., Carrivick, J.L. and Brown, L.E. (2017) 'The Multitrophic Effects of Climate Change and Glacier Retreat in Mountain Rivers', *BioScience*, 67(10), pp. 897–911. Available at: https://doi.org/10.1093/biosci/bix107.

Franklin, S., Ahmed, O. and Williams, G. (2017) 'Northern Conifer Forest Species Classification Using Multispectral Data Acquired from an Unmanned Aerial Vehicle', *Photogrammetric Engineering & Remote Sensing*, 83, pp. 501–507. Available at: https://doi.org/10.14358/PERS.83.7.501.

Franklin, S.E. (2018) 'Pixel- and object-based multispectral classification of forest tree species from small unmanned aerial vehicles', *Journal of Unmanned Vehicle Systems*, 6(4), pp. 195–211. Available at: https://doi.org/10.1139/juvs-2017-0022.

Green, D.S. (2005) 'Adaptive strategies in seedlings of three co-occurring, ecologically distinct northern coniferous tree species across an elevational gradient', *Canadian Journal of Forest Research*, 35(4), pp. 910–917. Available at: https://doi.org/10.1139/x05-015.

Haghshenas, M. and Wood, L.J. (2024) 'Subalpine fir response to drought in northern British Columbia, Canada', *Forestry: An International Journal of Forest Research*, p. cpae052. Available at: https://doi.org/10.1093/forestry/cpae052.

Harsch, M.A. *et al* (2009) 'Are treelines advancing? A global meta-analysis of treeline response to climate warming', *Ecology Letters*, 12(10), pp. 1040–1049. Available at: https://doi.org/https://doi.org/10.1111/j.1461-0248.2009.01355.x.

Janitza, S., Celik, E. and Boulesteix, A.-L. (2018) 'A computationally fast variable importance test for random forests for high-dimensional data', *Advances in Data Analysis and Classification*, 12(4), pp. 885–915. Available at: https://doi.org/10.1007/s11634-016-0276-4.

Jiang, M. *et al* (2023) 'Seeing Trees from Drones: The Role of Leaf Phenology Transition in Mapping Species Distribution in Species-Rich Montane Forests', *Forests*, 14(5). Available at: https://doi.org/10.3390/f14050908.

Klaar, M.J. *et al* (2015) 'Vegetation succession in deglaciated landscapes: implications for sediment and landscape stability', *Earth Surface Processes and Landforms*, 40(8), pp. 1088–1100. Available at: https://doi.org/https://doi.org/10.1002/esp.3691.

Koch, J., Menounos, B. and Clague, J.J. (2009) 'Glacier change in Garibaldi Provincial Park, southern Coast Mountains, British Columbia, since the Little Ice Age', *Global and Planetary Change*, 66(3), pp. 161–178. Available at: https://doi.org/https://doi.org/10.1016/j.gloplacha.2008.11.006.

Little, R.L., Peterson, D.L. and Conquest, L.L. (1994) 'Regeneration of subalpine fir (Abieslasiocarpa) following fire: effects of climate and other factors', *Canadian Journal of Forest Research*, 24(5), pp. 934–944. Available at: https://doi.org/10.1139/x94-123

© The Author(s) or their Institution(s)

Lloyd, A.H. and Bunn, A.G. (2007) 'Responses of the circumpolar boreal forest to 20th century climate variability", *Environmental Research Letters*, 2(4). Available at: https://doi.org/10.1088/1748-9326/2/4/045013.

Mathews, W.H. (1958) 'Geology of the mount garibaldi map-area, southwestern British Columbia, Canada: part I: igneous and metamorphic rocks', *GSA Bulletin*, 69(2), pp. 161–178. Available at: https://doi.org/10.1130/0016-7606(1958)69[161:GOTMGM]2.0.CO;2.

Milner, A., Brown, L. and Hannah, D. (2009) 'Hydroecological response of river systems to shrinking glaciers', *Hydrological Processes*, 23, pp. 62–77. Available at: https://doi.org/10.1002/hyp.7197.

Mood, B.J. and Smith, D.J. (2015) 'Holocene glacier activity in the British Columbia Coast Mountains, Canada', *Quaternary Science Reviews*, 128, pp. 14–36. Available at: https://doi.org/10.1016/j.quascirev.2015.09.002.

Norton *et al* (2025), unpublished

Nitschke, C.R. *et al* (2012) 'The influence of climate change, site type, and disturbance on stand dynamics in northwest British Columbia, Canada', *Ecosphere*, 3(1), p. art11. Available at: https://doi.org/10.1890/ES11-00282.1.

Pepin, N. *et al* (2015) 'Elevation-dependent warming in mountain regions of the world', *Nature Climate Change*, 5(5), pp. 424–430. Available at: https://doi.org/10.1038/nclimate2563.

Peterson, D., Peterson, D. and Ettl, G. (2002) 'Growth Responses of Subalpine Fir to Climatic Variability in the Pacific Northwest', *Canadian Journal of Forest Research-revue Canadienne De Recherche Forestiere - CAN J FOREST RES*, 32, pp. 1503–1517. Available at: https://doi.org/10.1139/x02-072.

Peterson, D.W. and Peterson, D.L. (2001) 'Mountain hemlock growth responds to climatic variability at annual and decadal time scales', *Ecology*, 82(12), pp. 3330–3345. Available at: https://doi.org/10.1890/0012-9658(2001)082[3330:MHGRTC]2.0.CO;2.

Province of British Columbia (2023) Forest and Fire Ecology Centre Strategic Plan 2023–2025. Victoria, BC: Government of British Columbia. Available at: https://www2.gov.bc.ca/assets/gov/environment/natural-resource-stewardship/nrs-climate-change/mitigation/ffec_strategic_plan_2023_25.pdf (Accessed: 27 May 2025).

Ramskogler, K. *et al* (2023) 'Primary succession and its driving variables – a sphere-spanning approach applied in proglacial areas in the upper Martell Valley (Eastern Italian Alps)', *Biogeosciences*, 20(14), pp. 2919–2939. Available at: https://doi.org/10.5194/bg-20-2919-2023.

Rice, S. *et al* (2012) 'Disturbance regimes at the interface of geomorphology and ecology', *Earth Surface Processes and Landforms*, 37(15), pp. 1678–1682. Available at: https://doi.org/10.1002/esp.3326.

Rounce, D.R. *et al* (2023) 'Global glacier change in the 21st century: Every increase in temperature matters', *Science*, 379(6627), pp. 78–83. Available at: https://doi.org/10.1126/science.abo1324.

© The Author(s) or their Institution(s)

637 Sakals, M. 2019. *Drones and Natural Resource Management* [Oral Presentation], 27 March, Bulkley
638 Valley Research Centre, Smithers.

639 Schiefer, F. *et al* (2020) 'Mapping forest tree species in high resolution UAV-based RGB-imagery by
640 means of convolutional neural networks', *ISPRS Journal of Photogrammetry and Remote Sensing*, 170,
641 pp. 205–215. Available at: https://doi.org/10.1016/j.isprsjprs.2020.10.015.

642 Strauss, S., Ruhland, C. and Day, T. (2009) 'Trends in soil characteristics along a recently deglaciated
643 foreland on Anvers Island, Antarctic Peninsula', *Polar Biology*, 32, pp. 1779–1788. Available at:
644 https://doi.org/10.1007/s00300-009-0677-3.

645 Swift, K. and Ran, S. (2012) 'Successional Responses to Natural Disturbance, Forest management, and
646 Climate Change in British Columbia's Forests', *BC Journal of Ecosystems and Management*, 13(1), pp.
647 1–23. Available at: http://jem.forrex.org/index.php/jem/article/viewFile/171/113

648 Trant, A.J. and Hermanutz, L. (2014) 'Advancing towards novel tree lines? A multispecies approach to
649 recent tree line dynamics in subarctic alpine Labrador, northern Canada', *Journal of Biogeography*, 41(6),
650 pp. 1115–1125. Available at: https://doi.org/10.1111/jbi.12287.

651 Uchytil, R.J. (1991) *Abies lasiocarp*a In: *Fire Effects Information System*. Available at:
652 https://www.fs.usda.gov/database/feis/plants/tree/abilas/all.html (Accessed 24 March 2025).

653 Vaillant, A. et al. (2024) 'NIRSpredict: a platform for predicting plant traits from near infra-red
654 spectroscopy', *BMC Plant Biology*, 24(1), p. 1100. Available at: https://doi.org/10.1186/s12870-024-
655 05776-0.

656 Wright, M.N. and Ziegler, A. (2017) 'ranger: A Fast Implementation of Random Forests for High
657 Dimensional Data in C++ and R', *Journal of Statistical Software*, 77(1), pp. 1–17. Available at:
658 https://doi.org/10.18637/jss.v077.i01.

659

660

661

662

663

664

665

Draft

© The Author(s) or their Institution(s)

666

667

668

669

670

671

672

673

674

675

676

677 **Supplementary Materials**

Draft

© The Author(s) or their Institution(s)

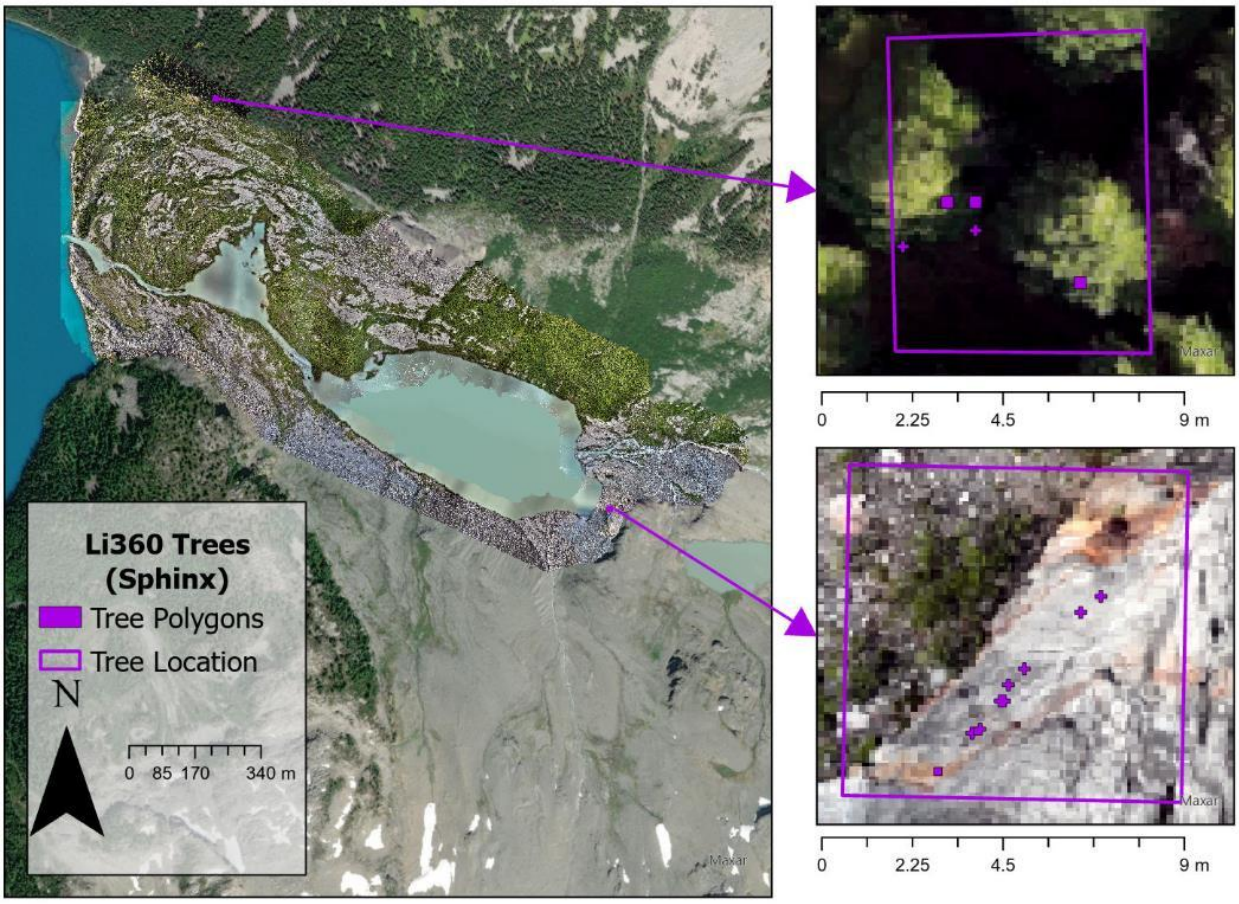


Figure S1. Illustration of issues found for this site with automated segmentation of trees in Sphinx Bay. Automated segmentation of trees resulted in small polygons both within trees and within abiotic terrain.

Table S1: Average band values within 1 standard deviation of conifers in the unguided dataset. Significant overlap is present in the spectral bands, with most bands in both datasets sharing over 70% of

© The Author(s) or their Institution(s)

overlap. The least overlap is found in Sphinx Bay, with 36.8% of overlap in elevation, 39.2% in slope, and 41.1% in near-infrared, and 50.1% in red-edge. In Sentinel Bay, the least overlap was found in Blue and in Red-2 (the red band from the multispectral camera).

Sentinel Unguided Dataset										
Band	**Red**	**Green**	**Blue**	**Green-2**	**Red-2**	**Red-Edge**	**Near-Infrared**	**Elevation**	**Slope**	**Aspect**
subalphine fir	12690 - 27932	15862 - 31718	7770 - 19789	7543 - 16582	3010 - 8522	16662 - 35305	18689 - 39390	1451 - 1470	10 - 51	74 - 282
mountain hemlock	13861 - 25915	17318 - 30876	7861 - 15739	8479 - 16070	3299 - 6951	20558 - 37261	23283 - 41571	1454 - 1471	9 - 45	59 - 284
overlap	13861 - 25915	17318 - 30876	7861 - 15739	8479 - 16070	3299 - 6951	20558 - 35305	23283 - 39390	1454 - 1470	10 - 45	74 - 282
overlap (%)	79.1	85.5	65.5	84	66.3	71.6	70.4	80	83.3	92.4
Sphinx Unguided Dataset										
Band	**Red**	**Green**	**Blue**	**Green-2**	**Red-2**	**Red-Edge**	**Near-Infrared**	**Elevation**	**Slope**	**Aspect**
subalpine fir	14997 - 36060	18334 - 39466	8450 - 25426	8874 - 20681	4809 - 14725	11962 - 27917	11397 - 26693	1465 - 1504	10 - 37	103 - 289
mountain hemlock	14857 - 33015	18201 - 36641	7473 - 21882	8609 - 18677	3705 - 11971	14821 - 38086	14163 - 41862	1447 - 1486	17 - 61	70 - 277
overlap	14997 - 33015	18334 - 36641	8450 - 21882	8874 - 18677	4809 - 11971	14821 - 27917	14163 - 26693	1465 - 1486	17 - 37	103 - 277
overlap (%)	85	86.1	74.8	81.2	65	50.1	41.1	36.8	39.2	79.5

Draft

Table S2: Results of agglomerative clustering of cells in the guided dataset with cluster values between 3 and 6.

Sentinel Guided Dataset (mhl n = 1046; saf n = 2019)							
Cluster count	Species	Cluster 0	Cluster 1	Cluster 2	Cluster 3	Cluster 4	Cluster 5

© The Author(s) or their Institution(s)

3-cluster	mhl	273	404	369	-	-	-
3-cluster	saf	782	1103	134	-	-	-
3-cluster	total	1055	1507	503	-	-	-
4-cluster	mhl	404	172	369	101	-	-
4-cluster	saf	1103	509	134	273	-	-
4-cluster	total	1507	682	503	374	-	-
5-cluster	mhl	6	398	369	101	172	-
5-cluster	saf	877	226	134	273	509	-
5-cluster	total	883	624	503	374	681	-
6-cluster	mhl	0	398	369	101	172	6
6-cluster	saf	635	226	134	273	509	242
6-cluster	total	635	624	503	374	681	248
Sphinx Guided Dataset (mhl n=2562; saf n=812)							
Cluster count	Species	Cluster 0	Cluster 1	Cluster 2	Cluster 3	Cluster 4	Cluster 5
3-cluster	mhl	1224	1014	324	-	-	-
3-cluster	saf	255	545	12	-	-	-
3-cluster	total	1479	1559	336	-	-	-
4-cluster	mhl	1014	325	324	899	-	-
4-cluster	saf	545	174	12	81	-	-
4-cluster	total	1559	499	336	980	-	-
5-cluster	mhl	325	594	324	899	420	-
5-cluster	saf	174	237	12	81	308	-
5-cluster	total	499	831	336	980	728	-
6-cluster	mhl	594	420	324	899	175	150
6-cluster	saf	237	308	12	81	120	54
6-cluster	total	831	728	336	980	295	204

703

704 **Table S3:** Band values of cell clusters in the guided dataset in Sentinel Bay within 1 standard deviation.

Dataset	Cluster	1	2	3	4	5	6	7	8	9	10
3-cluster	0	11558 - 19931	14146 - 22890	7817 - 14369	7037 - 11639	3382 - 5963	13285 - 22375	14872 - 23697	1453 - 1462	11 - 47	73 - 264
3-cluster	1	18281 - 25926	22737 - 29732	10418 - 20510	11104 - 14975	4716 - 8281	21568 - 29837	23879 - 32150	1453 - 1458	17 - 62	157 - 298

© The Author(s) or their Institution(s)

3-cluster	2	15470 - 22340	18716 - 26088	7421 - 12996	8483 - 11312	3498 - 4969	23006 - 31696	26184 - 35192	1507 - 1524	5 - 36	117 - 299
4-cluster	0	18281 - 25926	22737 - 29732	10418 - 20510	11104 - 14975	4716 - 8281	21568 - 29837	23879 - 32150	1453 - 1458	17 - 62	157 - 298
4-cluster	1	15476 - 20710	18127 - 23830	9354 - 15523	9079 - 12179	4270 - 6373	16707 - 23594	18011 - 24909	1453 - 1461	11 - 49	72 - 266
4-cluster	2	15470 - 22340	18716 - 26088	7421 - 12996	8483 - 11312	3498 - 4969	23006 - 31696	26184 - 35192	1507 - 1524	5 - 36	117 - 299
4-cluster	3	8530 - 14407	11207 - 16869	6731 - 10556	5573 - 8403	2768 - 4216	10601 - 16610	12331 - 18316	1453 - 1463	11 - 43	73 - 262
5-cluster	0	19023 - 27293	23221 - 30838	14151 - 22484	11260 - 15164	5574 - 9085	21181 - 26602	23784 - 28971	1454 - 1455	33 - 69	149 - 302
5-cluster	1	17909 - 23313	22488 - 27730	8410 - 14442	10909 - 14684	4347 - 6297	23826 - 32704	25573 - 35090	1455 - 1460	6 - 42	169 - 291
5-cluster	2	15470 - 22340	18716 - 26088	7421 - 12996	8483 - 11312	3498 - 4969	23006 - 31696	26184 - 35192	1507 - 1524	5 - 36	117 - 299
5-cluster	3	8530 - 14407	11207 - 16869	6731 - 10556	5573 - 8403	2768 - 4216	10601 - 16610	12331 - 18316	1453 - 1463	11 - 43	73 - 262
5-cluster	4	15476 - 20710	18127 - 23830	9354 - 15523	9079 - 12179	4270 - 6373	16707 - 23594	18011 - 24909	1453 - 1461	11 - 49	72 - 266
6-cluster	0	18494 - 24364	22558 - 28450	14436 - 18835	10935 - 13934	5526 - 7779	20780 - 25536	23725 - 28274	1454 - 1455	42 - 72	143 - 301
6-cluster	1	17909 - 23313	22488 - 27730	8410 - 14442	10909 - 14684	4347 - 6297	23826 - 32704	25573 - 35090	1455 - 1460	6 - 42	169 - 291
6-cluster	2	15470 - 22340	18716 - 26088	7421 - 12996	8483 - 11312	3498 - 4969	23006 - 31696	26184 - 35192	1507 - 1524	5 - 36	117 - 299
6-cluster	3	8530 - 14407	11207 - 16869	6731 - 10556	5573 - 8403	2768 - 4216	10601 - 16610	12331 - 18316	1453 - 1463	11 - 43	73 - 262
6-cluster	4	15476 - 20710	18127 - 23830	9354 - 15523	9079 - 12179	4270 - 6373	16707 - 23594	18011 - 24909	1453 - 1461	11 - 49	72 - 266
6-cluster	5	24177 - 30991	28074 - 33800	17760 - 27490	13683 - 16719	7179 - 10948	23166 - 28376	24274 - 30416	1454 - 1456	19 - 51	165 - 305

705

706

707

708 **Table S4:** Band values of cell clusters in the guided dataset in Sphinx Bay within 1 standard deviation.

Dataset	Cluster	1	2	3	4	5	6	7	8	9	10
3-cluster	0	18039 - 28081	20502 - 31495	10602 - 19836	9691 - 15731	4547 - 7253	24695 - 37367	25319 - 40337	1452 - 1462	16 - 43	85 - 310
3-cluster	1	9548 - 18419	12265 - 22376	5700 - 12096	6422 - 11301	2996 - 4879	15366 - 29037	16487 - 32289	1453 - 1462	11 - 34	54 - 282
3-cluster	2	22162 - 30276	24164 - 32253	13577 - 22166	10539 - 15065	5239 - 8556	40675 - 61916	49739 - 66645	1448 - 1451	15 - 37	-19- 195
4-cluster	0	9548 - 18419	12265 - 22376	5700 - 12096	6422 - 11301	2996 - 4879	15366 - 29037	16487 - 32289	1453 - 1462	11 - 34	54 - 282
4-cluster	1	21456 - 32216	25036 - 35581	11757 - 22804	12802 - 17967	5872 - 8444	27417 - 41623	25974 - 42116	1456 - 1466	12 - 39	60 - 283
4-cluster	2	22162 - 30276	24164 - 32253	13577 - 22166	10539 - 15065	5239 - 8556	40675 - 61916	49739 - 66645	1448 - 1451	15 - 37	-19 - 195
4-cluster	3	17621 - 24654	19659 - 27949	10510 - 17828	9141 - 13557	4420 - 6099	24198 - 34312	25077 - 39340	1452 - 1457	19 - 45	100 - 321

© The Author(s) or their Institution(s)